Biosensors and Bioelectronics 72 (2015) 230–236

Contents lists available at ScienceDirect

Biosensors and Bioelectronics

journal homepage: www.elsevier.com/locate/bios

Fast and sensitive detection of an anthrax biomarker using SERS-based solenoid microfluidic sensor

Rongke Gao [a,1], Juhui Ko [a,1], Kiweon Cha [b], Jun Ho Jeon [b], Gi-eun Rhie [b], Jonghoon Choi [a], Andrew J. deMello [c,*], Jaebum Choo [a,*]

[a] Department of Bionano Technology, Hanyang University, Ansan 426-791, South Korea
[b] Division of High-Risk Pathogen Research, Center for Infectious Diseases, National Institute of Health, Cheongju 363-951, South Korea
[c] Department of Chemistry and Applied Biosciences, Institute of Chemical and Bioengineering, ETH Zürich, Vladimir Prelog Weg 1, 8093 Zürich, Switzerland

ARTICLE INFO

Article history:
Received 3 March 2015
Received in revised form
30 April 2015
Accepted 4 May 2015
Available online 6 May 2015

Keywords:
Anthrax
Surface-enhanced Raman scattering
Microfluidics
Solenoid
Poly-γ-D-glutamic acid

ABSTRACT

We report the application of a fully automated surface-enhanced Raman scattering (SERS)-based solenoid-embedded microfluidic device to the quantitative and sensitive detection of anthrax biomarker poly-γ-D-glutamic acid (PGA) in solution. Analysis is based on the competitive reaction between PGA and PGA-conjugated gold nanoparticles with anti-PGA-immobilized magnetic beads within a microfluidic environment. Magnetic immunocomplexes are trapped by yoke-type solenoids embedded within the device, and their SERS signals were directly measured and analyzed. To improve the acccuracy of measurement process, external standard values for PGA-free serum were also measured through use of a control channel. This additional measurement greatly improves the reliability of the assay by minimizing the influence of extraneous experimental variables. The limit of detection (LOD) of PGA in serum, determined by our SERS-based microfluidic sensor, is estimated to be 100 pg/mL. We believe that the defined method represents a valuable analytical tool for the detection of anthrax-related aqueous samples.

1. Introduction

Anthrax is an acute disease caused by the gram-positive bacterium *Bacillus anthracis* (Little and Ivins, 1999; Turk, 2007; Boyden and Dietrich, 2006; Park et al., 2002). Infection occurs only when spores enter the body by inhalation or consumption of contaminated food or water. If the spores are active, bacteria multiply, spread, produce toxins and ultimately cause severe illnesses. Over the past two decades, the potential use of anthrax as a biological weapon by terrorists has become an increasingly significant threat. For this reason, the Center for Disease Control and Prevention of the United States classifies *B. anthracis* as a Tier 1 select agent with high bioterrorism potential (Skyberg, 2014). Accordingly, rapid and sensitive methods for the detection of anthrax *in vivo* are urgently needed for both early diagnosis and successful treatment after exposure. Recently, it has been reported that the *B. anthracis* capsule is composed of poly-γ-D-glutamic acid (PGA), which is closely associated with the pathogenesis of the *B. anthracis* infection since it protects bacilli from immune surveillance (Scorpio et al., 2007; Jang et al., 2013). Consequently, the PGA capsule can be used as a target marker for the detection of *B. anthracis*.

Various detection methods, such as immunofluorescence microscopy (Dal Molin et al., 2006; Zornetta et al., 2010), enzyme-linked immunoassays (ELISA) (Dominguez-Castillo et al., 2012; Seo et al., 2015) and polymerase chain reaction (PCR)-based assays (Euler et al., 2013; Seiner et al., 2013) have been used for the direct identification of *B. anthracis*. Unfortunately, these methods have significant technical drawbacks such as poor limits of detection, extensive sample pretreatment and unacceptably long assay times, which make them undesirable for both laboratory and in-the-field implementation. Accordingly, there is a demonstrated and pressing need for rapid, direct and sensitive detection of *B. anthracis* in humans.

Surface-enhanced Raman scattering (SERS) detection is an emerging read-out technique that allows the sensitive, selective and fast detection of biomarker molecules (Porter et al., 2008; Driskell et al., 2005; Li et al., 2008; Han et al., 2008). For this reason, the application of SERS-based techniques for fast and sensitive disease diagnosis has become increasingly popular. To date, variety of biomarkers has been quantitatively probed using SERS-based immunoassays. One of the most popular SERS assay platforms is based on a sandwich immunoassay containing

* Corresponding authors. Fax: +82 31 436 8188.
E-mail addresses: andrew.demello@chem.ethz.ch (A.J. deMello), jbchoo@hanyang.ac.kr (J. Choo).
[1] These authors contributed equally to this work.

http://dx.doi.org/10.1016/j.bios.2015.05.005
0956-5663/

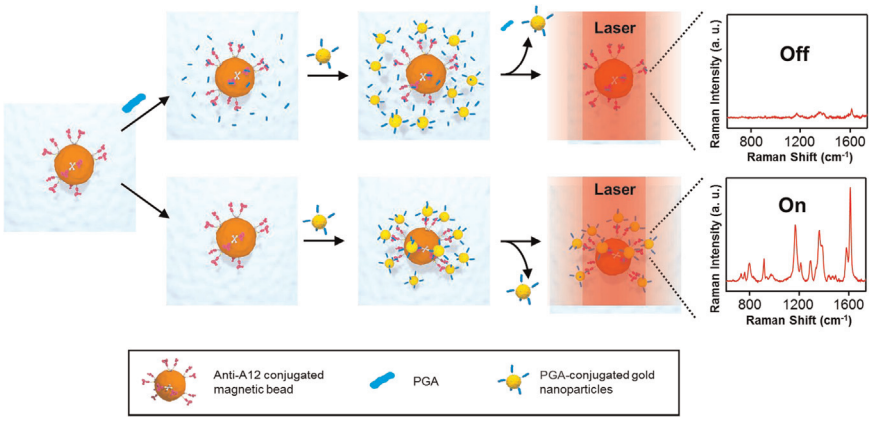

Fig. 1. Schematic illustration of the SERS-based competitive immunoassay for quantification of PGA marker in serum. PGA-conjugated AuNPs will not bind on anti-A12 conjugated magnetic bead in the presence of PGA, resulting in a weak SERS intensity (top). In contrast, strong SERS signals are observed without PGA (bottom).

primary antibody-conjugated magnetic beads (as substrates) and secondary antibody-conjugated SERS nano-tags (as probes) (Lee et al., 2011; Gong et al., 2007; Chon et al., 2009, 2011). Here, antigen is sandwiched between the two antibodies, with the binding affinity between the antibody and antigen defining assay sensitivity. Unfortunately, this sandwich assay protocol suffers from a cross reactivity and long assay time (Porter et al., 2008; Chon et al., 2009).

To resolve these issues, SERS-based competitive immunoassays have been developed (Chon et al., 2014). For example, we recently reported the feasibility of SERS-based competitive immunoassay using anti-PGA conjugated magnetic beads PGA antigen-conjugated gold nanoparticles (AuNPs) for the fast and reproducible detection of PGA markers (Ko et al., 2015). A schematic illustration of the SERS-based competitive immunoassay process for PGA is shown in Fig. 1. AuNPs conjugated with PGA antigens are utilized as "SERS nano-tags" and anti-PGA-immobilized magnetic beads as supporting substrates. When free PGA target antigens and PGA-conjugated AuNPs are mixed with magnetic beads, they undergo competitive reaction with the antibodies on magnetic beads. After the reaction is complete, immunocomplexes are isolated by a magnetic bar, and then unreacted free PGA target antigens and PGA-conjugated AuNPs removed. The SERS signals of the immunocomplexes are then measured. As more PGA antigens is added, the surface loading of bound PGA increases, and less PGA-conjugated AuNPs remain on the magnetic beads, resulting in decrease of SERS intensity of immunocomplexes.

Nonetheless, such SERS-based competitive immunoassays using conventional microtubes and magnetic bars raise technical issues: such as an inhomogeneous distribution of magnetic immunocomplexes on the wall of a microtube, the requirement for manual washing steps and magnetic field intensities. To address these drawbacks, we herein implement a competitive immunoassay into a solenoid-embedded dual-channel microfluidic device containing both sensing and control channels, for the rapid immunoassay of PGA trace markers in human serum. This proposed method is expected to be a useful analytical tool for the fast detection of anthrax in solution.

2. Experimental

2.1. Materials and reagents

Gold (III) chloride trihydrate (> 99.9%), sodium citrate dehydrate (99%), bovine serum albumin (BSA), ethanolamine, Rhodamine 6G (R6G), Rhodamine B (RB), dihydrolopic acid (DHLA), 1-ethyl-3-(3-dimethylaminopropyl) carbodiimide (EDC) and N-hydroxysuccinimide (NHS) were purchased from Sigma-Aldrich, and used without further purification. Poly-γ-D-glutamic acid (PGA) and A-12 antibodies were supplied by the Korea Centers for Disease Control and Prevention. Biotin-PEG 5000-NHS, used for the bio-functionalization of capture magnetic beads, was purchased from Santa Cruz Biotechnology (Santa Cruz, CA, USA). Streptavidin-coated magnetic beads and malachite green isothiocyanate (MGITC) were purchased from Invitrogen Corporation (Carlsbad, CA, USA). The average diameter of the magnetic beads was 1 μm. SeraSub® synthetic serum was obtained from CST Technologies. Phosphate-buffered saline (PBS) solutions containing 0.05% Tween-20 (v/v) at pH 7.4 were prepared using standard methods. Polydimethylsiloxane (PDMS, Sylgard 184 Silicone. Elastomer Kit) was purchased from Dow Corning. Deionized water was purified using a Milli-Q water purification system (Millipore Corporation, Billerica, MA, USA).

2.2. Preparation of PGA-conjugated gold nanoparticles (AuNPs)

AuNPs were synthesized using the citrate-reduction method reported by Frens (1972). In brief, 100 mL of 0.01% gold chloride trihydrate solution was heated to boiling, and 1.0 mL of 1% trisodium citrate dehydrate solution added under vigorous stirring. Within a few seconds, the color of the solution changed from faintly blue to brilliant red, indicating the formation of AuNPs. After the mixture was boiled for 20 min, heat was removed and the solution was stirred for 1 h. TEM images and size distributions determined by the dynamic light scattering measurements have been displayed in Fig. S1. AuNPs show homogeneous size distribution, and the average particle size is estimated to be 41.5 ± 3.5 nm. To prepare SERS-active nanoprobes, 0.5 μL of 0.1 mM MGITC was added to 1.0 mL of 0.1 nM AuNPs, and the mixture was reacted for 1 h under stirring. A 2.5 μL of 0.1 mM DHLA was first added into 1 mL of Au NPs solution. After incubation for 1 h, 2.5 μL of 0.1 mM EDC and NHS were added and allowed to react with the activated the –COOH terminal groups of the DHLA molecules for 15 min. Finally, 1.0 μL of 1 mg/mL PGA was added to the NHS-activated AuNPs and reacted for 1 h. Unreacted NHS groups on the surface of the AuNPs were deactivated by adding 2.5 μL of 0.1 mM ethanolamine for 20 min. Nonspecific binding chemicals were removed through centrifugation, and the remaining nanoprobes were washed with PBS buffer solution three times.

2.3. Preparation of PGA antibody-conjugated magnetic beads

For the bioconjugation of magnetic beads, 0.1 mL of Biotin-PEG

5000-NHS (4 mg/mL) was mixed with 0.1 mL of A-12 PGA antibody (2 mg/mL), and was reacted overnight with gentle mixing at 4 °C. Then, 0.2 mL of streptavidin-coated magnetic beads (1 mg/mL) was added to this solution, and the mixture stirred for 1 h at room temperature. After incubation, the tube was placed on a magnet for 4 min and the supernatant solution removed. A-12 antibody-conjugated magnetic beads were washed three times with PBS buffer, and were dissolved in 0.2 mL of PBS buffer.

2.4. Fabrication of the solenoid-embedded PDMS microfluidic channel

A solenoid-embedded PDMS microfluidic channel was fabricated by standard soft lithography and rapid prototyping methods. A positive SU-8 50-100 photoresist (Microchem Corp.) mold was fabricated on a silicon wafer using a transparent mask patterned at a resolution 20,000 dpi using a laser printer (Duffy et al., 1998). The pattern including groove-shaped mixers was transferred to a silicon wafer through a high-resolution photomask (AutoCAD 2008/AutoDesk Inc., OR, U.S.A.). Subsequently, PDMS prepolymer and curing agent (Sylgard 184, Dow Corning) were mixed in a 10:1 ratio (w/w) and then degassed with a vacuum pump. Groove-shaped mixers were incorporated into the channel to increase the mixing efficiency (Stroock et al., 2002; DeMello, 2006). Subsequently, two homemade mini-solenoids were placed alongside the channel. The PDMS prepolymer was poured into the mold and compressed using an aluminum disk. The prepolymer was cured at 70 °C for 2 h in a vacuum oven, and the structured layer then peeled off from the master mold. Inlet and outlet holes for fluidic access were punched in the structured replica. After treatment in an oxygen plasma, the bottom layer of structured PDMS substrate was aligned onto a glass slide to form a irreversible bond. All channels were 250 μm wide and 100 μm deep.

Solenoids were fabricated by coiling 26 turns of copper wire (insulated with lacquer and 300 μm in diameter) on a ferroelectric yoke of 1 mm diameter, 9 mm height, 4 mm width, and containing a 1 mm gap between the channels. Current was supplied using an Agilent E3631A (Agilent Technologies, Inc., U.S.A.) power source. The maximum magnetic force between the N and S poles of the solenoid was estimated to be approximately 27 mT. Such a field intensity is sufficient to trap the magnetic immunocomplexes on the channel wall. Finally, the upper PDMS layer for collecting waste solutions was aligned with the solenoid-embedded bottom layer using an oxygen plasma as shown in Fig. S2.

2.5. Image measurements and SERS detection

Bright field images of captured immunocomplexes were measured using an Olympus IX71 inverted microscope containing a DP20 CCD camera (Olympus Co., Japan). Precision syringe pumps (PHD 2000, Harvard Apparatus, USA), 1 mL Norm-Ject Plastic syringes (Henke-Sass Wolf GmbH, Germany), 32 mm, 22 G needle (KOVAX-NEEDLE®, Korea Vaccine Co., Ltd., Seoul, Korea), and Tygon microbore tubing (ID=0.02 IN, Saint-Gobain PPL Corp.) were used to inject samples into the solenoid-embedded microfluidic channel. Fluorescence measurements were performed using an Olympus IX81 inverted microscope (Olympus Co., Japan). Images assessing mixing efficiency within the microfluidic channel were acquired and analyzed using Q-imaging software.

Raman spectra were obtained using a Renishaw inVia Raman microscope system. A Renishaw RL633 He–Ne laser operating at λ=632.8 nm with a power of 5 mW was employed as the excitation source. The Rayleigh line was removed from the obtained Raman signal through a holographic notch filter located in the collection path. Raman scattering was measured with a charge-coupled device (CCD) camera with a spectral resolution of 1 cm^{-1}. A 20× objective lens (numerical aperture=0.4) was used to focus a laser spot on the magnetic immunocomplexes in a solenoid-embedded microfluidic channel. The exposure time was 10 s and the laser spot size was 1 μm. Renishaw WiRE 4.0 software was used for both data acquisition and control. Fig. S3a displays the experimental setup for the SERS measurements of magnetic immunocomplexes in the microfluidic channel. The flow rates were controlled simultaneously using three micro-syringe pumps. Fig. S3b also shows the optical arrangement for focusing the laser on the capture area of the channel.

3. Results and discussion

3.1. Fabrication of the solenoid-embedded dual channel microfluidic sensor

To ensure the safe detection and analysis of hazardous materials, short assay times and accurate fluidic control are essential. Accordingly, we designed and fabricated a dual channel microfluidic device to perform the PGA immunoassay in an automated fashion. Fig. 2 illustrates the schematic design of the microfluidic device used in this study. The device consists of two parallel channel compartments: one for PGA sensing and the other for control measurements. The sensing channel assays serum for various concentrations of the PGA trace. Conversely, the control channel only detects PGA-free serum as an external standard. Both channels are also composed of three compartments in the vertical direction. In the first compartment of the sensing channel, serum including target trace PGA antigens and anti-PGA-conjugated magnetic beads were introduced into the channel via two inlets. In the second compartment, PGA-conjugated AuNPs were introduced into the channel via the inlet located in the middle part of the device. Here, PGA antigens and PGA-conjugated AuNPs undergo competitive reaction with the antibodies on magnetic beads under flow conditions. As shown in Fig. 3b, a staggered herringbone groove-shaped mixer was incorporated into the channel to improve mixing efficiency. The third compartment acts to trap and detect magnetic immunocomplexes. To achieve effective trapping of the magnetic beads in the stream, two yoke-type mini-solenoids (Afshar et al., 2011; Han et al., 2011; Liu et al., 2007) were arranged at the end of each channel. After trapping the immunocomplexes, PGA free serum was introduced from the inlet, located in the middle part of the device, to wash out unbound PGA antigens and AuNPs. Finally, the SERS signal was measured by focusing the laser beam within each microfluidic channel. In the case of the control measurement, the assay and SERS detection were performed using the same procedure.

3.2. Mixing evaluation of microfluidic channel using fluorescence microscope

Before the SERS-based quantitative analysis of PGA in the microfluidic channel, color measurements using a fluorescence microscope have been performed to evaluate the mixing efficiency of the groove-shaped mixer. Fig. 3 demonstrates the results of a mixing evaluation using a 3.6×10^{-3} M RB solution and a 6×10^{-5} M R6G. To find the optimum flow rate for fluorescence measurements, the aqueous stream flow rates were varied from 0.1 to 5.0 μL min^{-1} using the microsyringe pump. On the basis of direct image analysis, optimal flow rates were determined to be 1.0, 3.0, and 2.0 μL min^{-1} for inlet 1 (PGA antigens, PGA free serum and magnetic beads), inlet 2 (PGA-conjugated AuNPs) and inlet 3 (serum for washing), respectively. To improve the understanding of the mixing process, fluorescence profiles across the channel width were measured at four different positions in the channel.

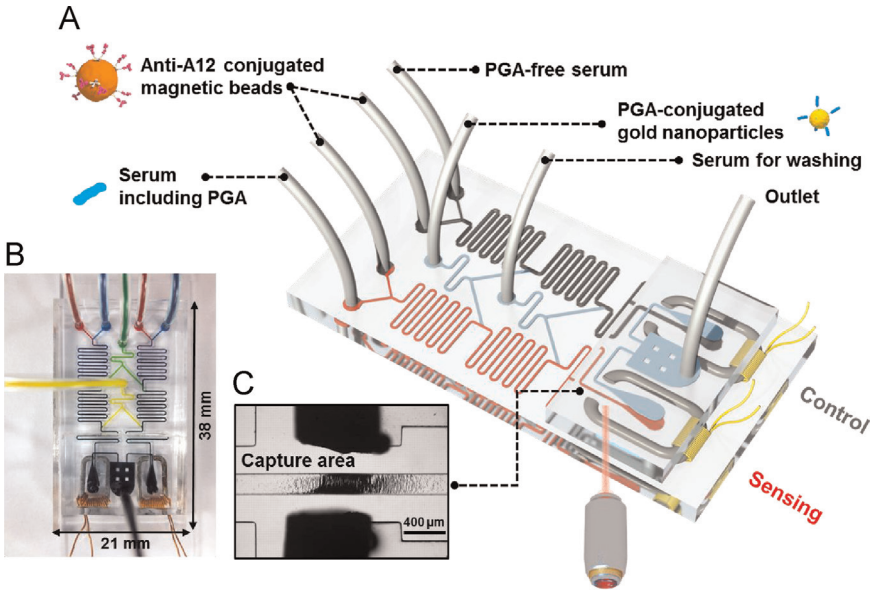

Fig. 2. (A) Schematic illustration of the solenoid-embedded dual channel microfluidic sensor for SERS-based competitive immunoassay. The sensor is composed of two parallel channels: one for PGA sensing (light gray) and the other for control (dark gray). (B) Optical images of the solenoid chip filled with four different colors of inks. (C) Photograph of the capture area for magnetic immunocomplexes.

Here, diffusion of the red fluorescence dye occurred from half of the channel (# i) to over the full channel (# ii). When the green fluorescence dye was introduced into the channel, it formed another laminar flow as shown in the fluorescence profile at # iii, with the green and red fluorescence dyes being completely mixed at channel position # iv. This demonstrates that mixing is efficiently accelerated by the staggered herringbone groove-shaped mixer.

3.3. SERS-based on-chip immunoassay

Fig. 4 displays a schematic representation of the experimental protocol for the SERS-based on-chip immunoassay. Herein, the assay process of the left channel (sensing) in Fig. 4 corresponds to the top picture of Fig. 1 ("Off"). On the other hand, the assay process of the right channel (control) in Fig. 4 corresponds to the bottom picture of Fig. 4 ("On"). When PGA-conjugated AuNPs were introduced into the channel from the inlet located in the middle part of the chip, strong SERS signals were measured for both the sensing and control channels. In the trapping and detection part of the channel, however, strong SERS signals were only observed in the control channel since all PGA-conjugated AuNPs are captured on magnetic beads. Conversely, the SERS intensity dramatically decreased when excess PGA antigens were introduced into the sensing channel because the loading density of AuNPs was decreased. AuNPs-loaded magnetic beads were collected for 3 min, and the final SERS signal was measured after unbound antigens and AuNPs were washed with PGA-free serum for 1 min. The total assay time was calculated to be between eight and ten minutes. In the SERS detection, the Raman intensity is enhanced by the amplification of the electromagnetic field resonance effects when the target species is trapped to the proximity of a metal nanoparticle.

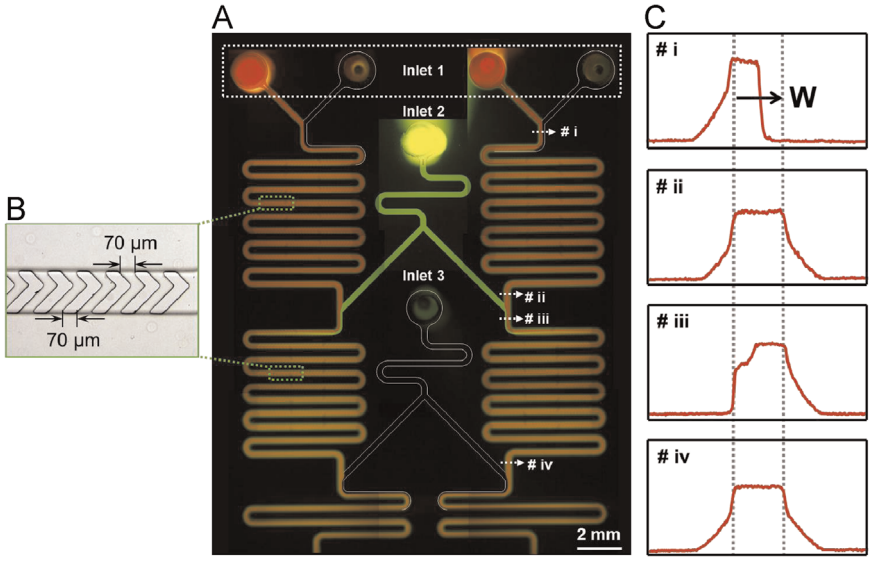

Fig. 3. Evaluation of mixing efficiency using 3.6×10^{-3} M RB and 6×10^{-5} M R6G solutions. (A) Fluorescent image of microfluidic channels. (B) Bright field image of the staggered herringbone groove-shaped mixer. (C) Corresponding fluorescence intensity profiles at locations indicated by dashed lines. *X* and *Y* axes denote the channel width and the relative fluorescence intensity, respectively.

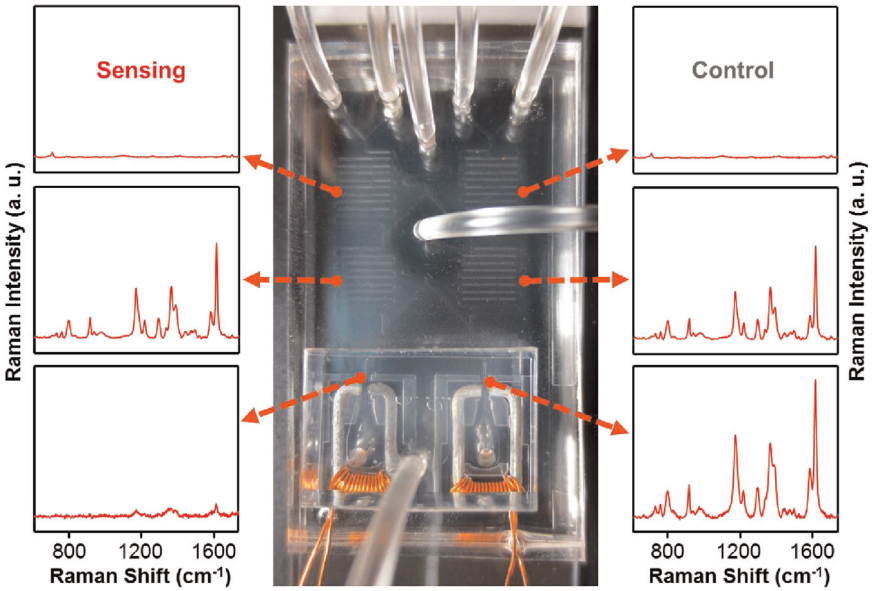

Fig. 4. Photograph of the solenoid microfluidic chip and SERS spectra at six different channel positions. The SERS signal was measured at the central point of the laminar flow.

It has been known that the formation of "hot spots" strongly enhances the SERS intensity (Kneipp et al., 1999; Otto et al., 1992). Two-dimensional nano-patterned substrate with high density "hot spots" has been popularly used to improve the detection limit. However, the inhomogeneity of the hot spot distribution on a planar substrate causes site dependence on the platform (Luo et al., 2014). To resolve this problem, SERS-based immunoassay using magnetic beads has been utilized in this work. This method does not use an immobilization procedure on a planar substrate; instead, it uses magnetic beads as antibody-supporting materials. Here, it is possible to obtain more reproducible results since the SERS signals are measured for the average "hot-spot" nanoparticle ensemble in solution (Chon et al., 2009; Huang et al., 2011). Furthermore, the detection sensitivity is greatly increased because the loading density of the capture antibody on a magnetic bead is dramatically increased on three-dimensional microspheres.

Fig. 5a shows images of magnetic imunocomplexes trapped inside the solenoid channel. The power supply was then used to control the magnetic field "on and off", and the image was recorded when the electrical power was switched on. This is a key advantage of electromagnets over permanent magnets within microfluidic systems since the yoke-type solenoid can be switched on/off rapidly (Siegel et al., 2006). The variation in SERS intensity after the capture of magnetic immunocomplexes was monitored as a function of time to determine the optimal capture time. It was observed that the capture process was essentially complete after three minutes since the SERS intensity at 1612 cm^{-1} plateaus as shown in Fig. 5b.

Fig. 6a illustrates SERS spectra collected from magnetic immunocomplexes for different PGA concentration-containing sera in the sensing solenoid channel. Here, the Raman peak entered at 1612 cm^{-1} was used for the quantitative evaluation of the PGA target trace. The intensity of the Raman peak decreases concomitantly with an increase in the concentration of PGA. As shown in Fig. 6b, a linear response (R^2=0.96) was achieved within the concentration range of 100 pg/mL to 100 μg/mL. However, one of the most important issues in quantitative analysis using SERS technique relates to experimental reproducibility. Many experimental variables, such as variations in laser power, distributions in particle size, localized heating and variable mixing times, could

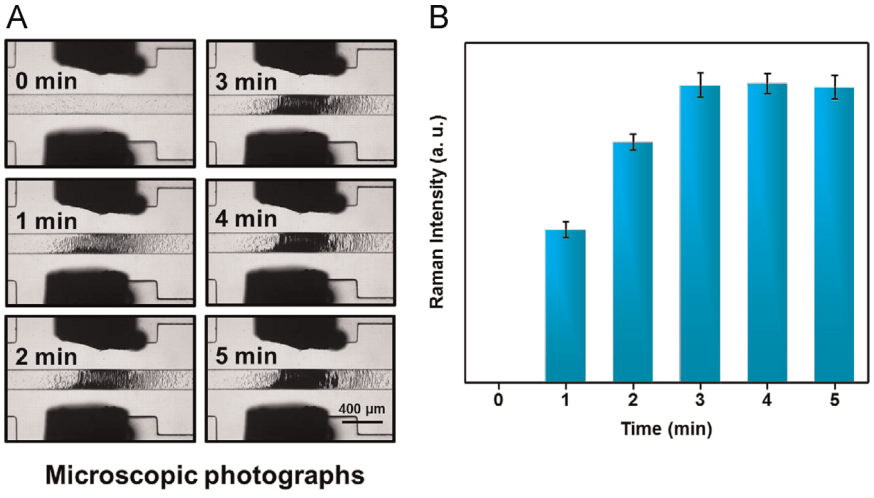

Fig. 5. (A) Micrographs of the trapped magnetic immunocomplexes in the channel over time, and (B) their relative SERS intensities at 1612 cm^{-1}. All error bars indicate standard deviations from three measurements.

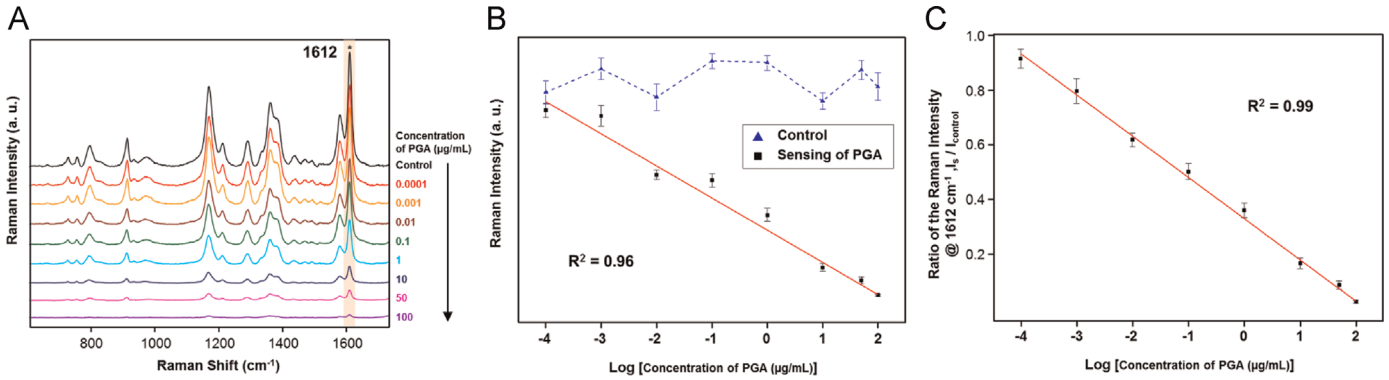

Fig. 6. (A) Concentration-dependent SERS spectra of PGA in the sensing channel. The concentrations ranged from 100 μg mL^{-1} to 1×10^{-4} μg mL^{-1}. (B) Variation of the SERS intensity at 1612 cm^{-1} as a function of PGA concentration in serum. Correlation coefficient, $R^2 = 0.96$. The upper dashed line shows the variation of the SERS intensity of the external standard, PGA-free serum, at 1612 cm^{-1} in the control channel. (C) Variation of peak intensity ratios of $I_{sensing}/I_{control}$ at 1612 cm^{-1} of SERS spectra as a function of PGA concentration. Correlation coefficient, $R^2 = 0.99$. All error bars indicate standard deviations from three measurements.

potentially affect reproducibility.

3.4. Reliability improvement using external standards in control channel

To resolve such a problem, the external standard value was measured using the control channel for each experiment (Numata et al., 2011; Pelletier., 2003; Walter et al., 2011; März et al., 2011). The use of an external standard eliminates the influence of almost all experimental variables when performing quantitative analyses. In the present work, the ratio of the SERS intensity of PGA-containing serum in the sensing channel to that of PGA-free serum (external standard) in the control channel was determined for different concentrations of PGA sera. In Fig. 6b, the upper dashed line reports the variation of the SERS intensity of the external standard at 1612 cm^{-1} in the control channel. When the variation of external standards has been considered for the quantitative analysis of PGA, the correlation coefficient increased from 0.96 to 0.99 as shown in Fig. 6c. All error bars in Fig. 6 report the standard deviations from a total of three measurements. The LOD assessed from the standard deviations was estimated to be 100 pg/mL. This value demonstrates that highly sensitive SERS-based detection of target trace PGA in serum is possible using the solenoid-embedded dual microfluidic channel device. To estimate the detection sensitivity of our SERS-based competitive PGA trace assay, ELISA data were collected and a dynamic curve determined in the range of 0.1–100 μg/mL. As shown in Fig. S4, the LOD determined by ELISA experiments was estimated to be 0.1–1.0 μg/mL.

4. Conclusions

In the present study, we have developed a novel SERS-based magnetic sensor for highly sensitive detection of anthrax biomarker PGA in human serum. For fast, sensitive and safe detection of such a hazardous material in human serum, we designed and fabricated a solenoid-embedded dual channel microfluidic device to perform the PGA immunoassay in an automated manner.

Quantitative assays for eight different concentrations of PGA trace in serum have been performed using the SERS-based microfluidic sensor. Here, PGA and PGA-conjugated AuNPs undergo competitive reaction with anti-PGA-immobilized magnetic beads in the microfluidic channel. Subsequently, magnetic immunocomplexes are trapped by yoke-type solenoids embedded in the channel, and their SERS signals were measured and analyzed. To improve the reliability for SERS measurements, the external standard values for PGA-free serum were measured each time using the control microfluidic channel. This greatly improves the reliability by minimizing the influence of most experimental variables.

The LOD determined by the SERS-based magnetic solenoid sensor was estimated to be 100 pg/mL. This low LOD value demonstrates that our SERS-based immunoassay is approximately three orders of magnitude more sensitive than corresponding ELISA-based methods. Accordingly, the proposed SERS-based magnetic solenoid microfluidic sensor technique, which possessing both high sensitivity and selectivity, shows significant potential for the quantitative and sensitive detection of hazardous materials in an automated manner.

Acknowledgments

The National Research Foundation of Korea supported this work (Grant number K20904000004-14A0500-00410). This work was partially supported by the Research Program from the Korea Centers for Disease Control and Prevention (Grant number 2014-E45002-00) and the Agency for Chemical & Biological Detection Research Center (CBDRC).

Appendix A. Supplementary material

Supplementary data associated with this article can be found in the online version at http://dx.doi.org/10.1016/j.bios.2015.05.005.

References

Afshar, R., Moser, Y., Lehnert, T., Gijs, M.A.M., 2011. Sens. Actuators B 154, 73–80.
Boyden, E.D., Dietrich, W.F., 2006. Nat. Genet. 38, 240–244.
Chon, H., Lee, S., Son, W.W., Oh, C.H., Choo, J., 2009. Anal. Chem. 81, 3029–3034.
Chon, H., Lee, S., Yoon, S.Y., Chang, S.I., Lim, D.W., Choo, J., 2011. Chem. Commun. 47, 12515–12517.
Chon, H., Lee, S., Yoon, S.Y., Lee, E.K., Chang, S.I., Choo, J., 2014. Chem. Commun. 50, 1058–1060.
Dal Molin, F., Tonello, F., Ladant, D., Zornetta, I., Zamparo, I., Di Benedetto, G., Zaccolo, M., Montecucco, C., 2006. EMBO J. 25, 5405–5413.
DeMello, A.J., 2006. Nature 442, 394–402.
Dominguez-Castillo, R.I., Verma, A., Amador-Molina, J.C., Sirota, L., Arciniega, J.L., 2012. Biologicals 41, 111–114.
Driskell, J.D., Kwarta, K.M., Lipert, R.J., Porter, M.D., Neill, J.D., Ridpath, J.F., 2005. Anal. Chem. 77, 6147–6154.
Duffy, D.C., McDonald, J.C., Schueller, O.J.A., Whitesides, G.M., 1998. Anal. Chem. 70, 4974–4984.
Euler, M., Wang, Y., Heidenreich, D., Patel, P., Strohmeier, O., Hakenberg, S., Niedrig,

M., Hufert, F.T., Weidmann, M., 2013. Anal. Chem. 85, 5562–5568.
Frens, G., 1972. Colloid Polym. Sci. 250, 736–741.
Gong, J.L., Liang, Y., Huang, Y., Chen, J.W., Jiang, J.H., Shen, G.L., Yu, R.Q., 2007. Biosens. Bioelectron. 22, 1501–1507.
Han, B., Choi, N., Kim, K.H., Lim, D.W., Choo, J., 2011. J. Phys. Chem. C 115, 6290–6296.
Han, X.X., Cai, L.J., Guo, J., Wang, C.X., Ruan, W.D., Han, W.Y., Xu, W.Q., Zhao, B., Ozaki, Y., 2008. Anal. Chem. 80, 3020–3024.
Huang, J., Kim, K.H., Choi, N., Chon, H., Lee, S., Choo, J., 2011. Langmuir 27, 10228–10233.
Jang, J., Cho, M., Lee, H.R., Cha, K., Chun, J.H., Hong, K.J., Park, J., Rhie, G.E., 2013. Biochim. Biophys. Acta 1830, 2804–2812.
Kneipp, K., Kneipp, H., Itzkan, I., Dasari, R.R., Feld, M.S., 1999. Chem. Rev. 99, 2957–2975.
Ko, J., Cha, K., Jeon, J., Rhie, G.E., Choi, J., Choo, J., 2015. Bull. Korean Chem. Soc. 36, 822–826.
Lee, M., Lee, S., Lee, J.H., Lim, H.W., Seong, G.H., Lee, E.K., Chang, S.I., Oh, C.H., Choo, J., 2011. Biosens. Bioelectron. 26, 2135–2141.
Li, T., Guo, L., Wang, Z., 2008. Biosens. Bioelectron. 23, 1125–1130.
Little, S.F., Ivins, B.E., 1999. Microbes Infect. 1, 131–139.
Liu, Y.J., Guo, S.S., Zhang, Z.L., Huang, W.H., Baigl, D., Chen, Y., Pang, D.W., 2007. J. Appl. Phys. 102, 084911.
Luo, S.C., Sivashanmugan, K., Liao, J.D., Yao, C.K., Peng, H.C., 2014. Biosens. Bioelectron. 61, 232–240.
März, A., Mönch, B., Rösch, P., Kiehntopf, M., Henkel, T., Popp, J., 2011. Anal. Bioanal. Chem. 400, 2755–2761.
Numata, Y., Iida, Y., Tanaka, H., 2011. J. Quant. Spectrosc. Radiat. 112, 1043–1049.
Otto, A., Mrozek, I., Grabhorn, H., Akemann, W., 1992. J. Phys. Condens. Matter 4, 1143–1212.
Park, J.M., Greten, F.R., Li, Z.W., Karin, M., 2002. Science 297, 2048–2051.
Pelletier, M.J., 2003. Appl. Spectrosc. 57, 20–42.
Porter, M.D., Lipert, R.J., Siperko, L.M., Wang, G., Narayana, R., 2008. Chem. Soc. Rev. 37, 1001–1011.
Scorpio, A., Chabot, D.J., Day, W.A., O'brien, D.K., Vietri, N.J., Itoh, Y., Mohamadzadeh, M., Friedlander, A.M., 2007. Antimicrob. Agents Chemother. 51, 215–222.
Seiner, D.R., Colburn, H.A., Baird, C., Bartholomew, R.A., Straub, T., Victry, K., Hutchison, J.R., Valentine, N., Bruckner-Lea, C.J., 2013. J. Appl. Microbiol. 114, 992–1000.
Seo, S.H., Lee, Y.R., Jun, H.J., Hwang, Y.R., Park, P.G., Ahn, D.R., Han, K.C., Rhie, G.E., Hong, K.J., 2015. Biosens. Bioelectron. 64, 69–73.
Siegel, A.C., Shevkoplyas, S.S., Weibel, D.B., Bruzewicz, D.A., Martinez, A.W., Whitesides, G.M., 2006. Angew. Chem. Int. Ed. 45, 6877–6882.
Skyberg, J.A., 2014. Curr. Top. Med. Chem. 14, 2115–2126.
Stroock, A.D., Dertinger, K.W., Ajdari, A., Mezic, I., Stone, H.A., Whiteside, G.M., 2002. Science 295, 647–651.
Turk, B.E., 2007. Biochem. J. 402, 405–417.
Walter, A., März, A., Schumacher, W., Rösch, P., Popp, J., 2011. Lab Chip 11, 1013–1021.
Zornetta, I., Brandi, L., Janowiak, B., Dal Molin, F., Tonello, F., Collier, R.J., Montecucco, C., 2010. Cell. Microbiol. 12, 1435–1445.